Impurity-induced phonon disordering in $Cd_{1-x}Zn_xTe$ ternary alloys

D. N. Talwar
*Solid State Electronics Directorate, Wright Laboratories, Wright Patterson Air Force Base, Ohio 45433-6543 and Department of Physics, Indiana University of Pennsylvania, Indiana, Pennsylvania 15705-1087**

Z. C. Feng
Department of Physics, National University of Singapore, Singapore 0511

P. Becla
Francis Bitter National Magnet Laboratory, Massachusetts Institute of Technology, Cambridge, Massachusetts 02139
(Received 7 May 1993)

A comprehensive study of impurity-induced phonon disordering in $Cd_{1-x}Zn_xTe$ alloys is reported for a variety of samples (with composition ranging from $x=0.005-0.5$, and 1) by using far-infrared reflectivity and Raman-scattering spectroscopy. Substantial differences were noted among the various published values for the optical-phonon frequencies versus x. Contrary to an earlier Raman study on molecular-beam-epitaxy grown $Cd_{1-x}Zn_xTe/GaAs$ films, our results yield increases in the numbers of both the CdTe- and ZnTe-like TO phonons with x. A modified random-element isodisplacement model provides excellent fits to the optical phonons. The effects of impurity-induced phonon disordering are studied, within the band mode region, by using an average-t-matrix formalism. Unlike earlier speculations in which a gap mode in ZnTe:Cd lies near $\sim 140-145$ cm^{-1}, our theory predicts it to be at a higher frequency, ~ 153 cm^{-1}. Group-theoretical analysis suggests that the gap mode exhibits a triply degenerate vibrational state and it can be detected both by IR absorption and Raman-scattering spectroscopy.

I. INTRODUCTION

Considerable efforts have been made in recent years to evaluate the basic properties of mixed II-VI compounds for applications in photovoltaic, photoconductive, and infrared (IR) detection devices. Earlier, narrow-band-gap mercury cadmium telluride (MCT) was used as an epilayer in fabricating high-performance optical devices.[1,2] However, this material suffers from serious drawbacks related to the poor lattice stability of its alloys. The lattice instability is caused primarily by the incorporation of Cd which weakens the Hg-Te bond.[3–5] Since the material is not tolerant or resilient to stress it can cause substantial variations in stochiometery. Stress may also be caused by simple processes such as oxidation, or reactions with metals, and/or by mechanical damage. The observed loss of Hg from MCT at elevated temperatures is thought to be as a result of one of the above processes. We mentioned that a small deviation ($\sim 0.1\%$) in stochiometry may result in native defects (e.g., vacancies, antisites, etc.) with concentrations as high as 10^{19} cm^{-3}. In MCT the native defects affect the transport properties and hence the device performance of IR photodetectors. Since the epitaxial layers used in IR detector arrays depend critically upon the quality of the surface and on the substrate, considerable interest has been stimulated to search for more stable materials for optical devices.

Theoretical calculations[6,7] made in recent years have indicated that the weak Hg-Te bond can be strengthened if alloyed with ZnTe instead of CdTe. However, the high segregation coefficients and large mercury vapor pressures at high temperature associated with the liquidus have indicated unfavorable conditions for the growth of homogeneous single crystals of $Hg_{1-x}Zn_xTe$ over the extended composition range.[8] In evaluating the characteristics of other members of the II-VI series our total-energy calculations[7] suggest that the Cd-Te bond in $Cd_{1-x}Zn_xTe$ is more stable than the Hg-Te bond in $Hg_{1-x}Zn_xTe$. Like other ternary compounds, $Cd_{1-x}Zn_xTe$ offers a large tunability with x for both the lattice parameter and for the band gap. It is at the value $x=0.04$ that $Cd_{1-x}Zn_xTe$ is lattice matched to $Hg_{0.78}Cd_{0.22}Te$ for the infrared detector applications. Although several studies[1,2] have been performed in recent years to understand the electronic properties (e.g., band-structure, defect-induced deep-electronic states, etc.) of $Cd_{1-x}Zn_xTe$ very little attention is paid for the optical examination of its dynamical behavior. We strongly believe that such a study of lattice dynamics is important to illustrate many fundamental aspects related to the crystal stability through the bonding mechanism.

In ternary compounds an excellent illustration of lattice dynamics can be obtained by using infrared (IR) reflectance and Raman-scattering spectroscopy. In the 1970s, three research groups[9–11] studied the variation of optical phonons as a function of x in $Cd_{1-x}Zn_xTe$ alloys at 300 and 80 K. All confirmed the two-mode behavior in $Cd_{1-x}Zn_xTe$ with nearly identical plots for the compositional dependence of ZnTe- and CdTe-like TO and LO phonons. The two-mode behavior is typical of mixed crystals for which the optical-phonon bands of pure materials do not overlap and where, near the extremes of the composition range, the localized mode of the minority ions lies well outside the restrahlen peak of the host crys-

tal. The authors of Refs. 9–11 showed the remarkable result stated by Vodop'yanov *et al.*; unlike every other two-mode system studied at the time in which one mode's TO frequency increases with x and the other decreases, in $Cd_{1-x}Zn_xTe$ both frequencies grow with x. The latest available compendium of II-VI ternary compounds[12] still shows no other compound with this behavior. However, Olego, Raccah, and Faurie[13] in a more recent work, obtained different results for the phonon frequencies for molecular-beam-epitaxy-grown $Cd_{1-x}Zn_xTe$/GaAs films than those reported by Perkowitz *et al.*[14] for $Cd_{1-x}Zn_xTe$ alloys. The authors of Ref. 13 show an increase in the ZnTe-like TO phonons with x, whereas no variation is found in the CdTe-like TO phonons with composition. The frequencies of the local and gap modes are extrapolated to be ~ 174 and 145 cm^{-1}, respectively, for low compositions of Zn and Cd in $Cd_{1-x}Zn_xTe$.[13] On the other hand, the Raman and IR data of Perkowitz *et al.*[14] for $Cd_{1-x}Zn_xTe$ alloys show an increase in both the CdTe and ZnTe-like TO-phonon frequencies with x, and a higher value for the gap mode in ZnTe:Cd.

The purpose of the present paper is to re-examine the unique phonon mode behavior in $Cd_{1-x}Zn_xTe$ alloys by using far-infrared reflectivity, which emphasizes the TO modes, and Raman-scattering spectroscopy, which is superior for the LO modes. Comprehensive theoretical calculations are also presented for the disorder-induced phonons in $Cd_{1-x}Zn_xTe$ by using a phenomenological lattice-dynamical theory. Due to the complexity involved in the structural and potential disorder, first-principles calculations have not yet been fully evolved for treating the vibrational behavior of mixed crystals. Extended x-ray-absorption fine-structure (EXAFS) measurements[15] have, however, sparked considerable interest in determining the local structure. We have recently developed a simple bond orbital model[7] (BOM) and estimated the lattice relaxation and force variations caused by low concentrations of Zn (Cd) impurities in CdTe (ZnTe). This information will be incorporated in an average-t matrix (ATM) formalism[16–18] to understand the optical-phonon properties of mixed $Cd_{1-x}Zn_xTe$ alloys. The self-energy terms which arise in the formalism are calculated to first order in concentration x, and involve certain Green's functions which have been computed numerically for CdTe and ZnTe, using a rigid-ion model of a harmonic zinc-blende lattice.[19] It will be shown how the infrared absorption and Raman scattering are related to certain phonon Green's functions. In spite of the fact that we do not start with a realistic theory of phonons for the host crystals, the disorder-activated transverse-acoustic (DATA), longitudinal-acoustic (DALA), and optical (DAO) structures in ternary compounds are very well described by the ATM. The results of numerical calculations for the compositional dependence of the optical phonons in $Cd_{1-x}Zn_xTe$ are compared with the infrared and Raman-scattering data.[9–11] Unlike earlier speculations[9,13] for the gap-mode in ZnTe:Cd to lie near ~ 140–145 cm^{-1} our theory predicts it to be at a relatively higher ~ 153 cm^{-1} frequency. Group-theoretical analysis suggests that the gap mode exhibits a triply degenerate vibrational state and it should be detected both by IR absorption and Raman-scattering spectroscopy in samples with low Cd composition.

II. EXPERIMENT

A. Sample preparation

The $Cd_{1-x}Zn_xTe$ ternary alloys (with x ranging from 0.005–0.5) were prepared at the Francis Bitter National Magnet Laboratory, Massachusetts Institute of Technology, by reacting the 99.9999% pure elemental constituents in evacuated quartz tubes. The composition values x were calculated from the mass densities. These precast alloys were regrown by directional solidification in a Bridgman-Stockbarger–type crystal-growth furnace. The regrowth occurred at the rate of 1.2 mm/h in the furnace adiabatic zone with a temperature gradient of about 15°C/cm. The resulting boules were sliced perpendicular to the growth direction. The slices used for the infrared and Raman measurements were annealed at 600°C in a Cd-saturated atmosphere for about 5 d. Their surfaces were prepared by lapping, mechanical polishing, and etching in a bromine-methanol solution.

B. Infrared reflectivity spectra

The far-infrared (FIR) reflectivity measurements were performed by using a Fourier-transform spectrometer and a Golay detector for good signal-to-noise ratios between 50 and 350 cm^{-1}. Data were taken at near-normal incidence and at sample temperatures of 300, 80, and 20–30 K. Although the main features of the IR spectra did not change significantly between 80 and 20–30 K, small features sharpened noticeably at the lowest temperatures. Several representative sets of reflectivity spectra of $Cd_{1-x}Zn_xTe$ ($x=0.01$, 0.2, and 0.5) at low temperatures (20–80 K) were reported earlier.[14] In Fig. 1, we display the IR spectra at 300 K for $Cd_{1-x}Zn_xTe$ (with $x=1$, 0.5, 0.4, 0.3, 0.2, 0.1, and 0.005). For alloy semi-

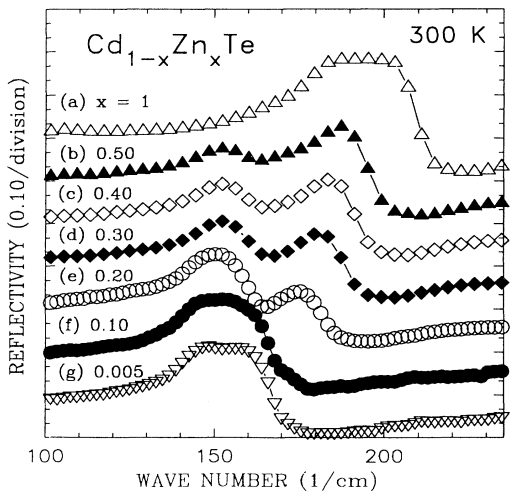

FIG. 1. Far-infrared reflectivity data for bulk $Cd_{1-x}Zn_xTe$ with compositions x of (a) 1, (b) 0.5, (c) 0.4, (d) 0.3, (e) 0.2, (f) 0.1, and (g) 0.005, measured at 300 K.

conductors, the IR spectra in the long-wavelength range are mainly modulated by the transverse-optical phonons. A perusal of Fig. 1 clearly shows a two-mode behavior between the two end members of the alloy. A single band between 160 and 215 cm^{-1} corresponds to an IR-active mode of pure ZnTe [Fig. 1(a)], whereas for $x=0.005$ a broadband for CdTe [Fig. 1(g)] is exhibited between 120 and 175 cm^{-1}. For samples with compositions $x=0.2-0.5$, ZnTe-like modes are observed at the higher-energy side and CdTe-like modes are seen at the lower-energy side, respectively, exhibiting clearly a two-mode behavior. For $x=0.1$, the ZnTe-like band is seen as a shoulder in Fig. 1(f) at the high-energy side of the strong CdTe characteristic band. For the sample with the lowest x, 0.005, we observe a weak but not clearly recognizable ZnTe-like shoulder [c.f. Fig. 1(g)]. Similar ZnTe-like shoulders (not displayed in Fig. 1) are observed for samples with $x=0.01$ and 0.03.

C. Raman spectra

Figure 2 displays Raman spectra recorded at 80 K for nine $Cd_{1-x}Zn_xTe$ alloy (with $x=0.005-0.5$, and 1.0) samples over the frequency range 100–440 cm^{-1}. This range covers both the first- and second-order phonon features. Because of the (100) surface of our samples, only longitudinal-optical (LO) phonons are allowed in the Raman measurement geometry. However, a few TO modes do appear in Fig. 2. These features are attributed to the alloy disordering and/or to the slight deviation from the true backscattering geometry. For the sample with the lowest $x=0.005$ value [c.f. Fig. 2(i)] the CdTe-like mode LO_1 and the ZnTe-like model LO_2 are mixed together. The LO_2 mode appears as a weak shoulder at the high-energy side of the LO_1. As x increases to 0.01 the LO_1 and LO_2 modes are clearly resolved [c.f. Fig. 2(h)] and for $x=0.03$, these modes are well separated [see Fig. 2(g)]. However, in IR measurements the two types of phonon modes for these three samples are not clearly recognizable.

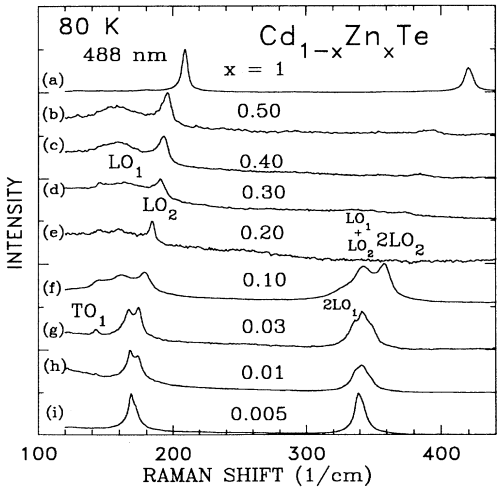

FIG. 2. Raman-scattering spectra of bulk $Cd_{1-x}Zn_xTe$ measured at 80 K with composition x of (a) 1, (b) 0.5, (c) 0.4, (d) 0.3, (e) 0.2, (f) 0.1, (g) 0.03, (h) 0.01, and (i) 0.005, and with the excitation of 488 nm from an Ar^+ laser. The laser power is 100 mW, focused on the sample surface with a spot size of about 0.2 mm.

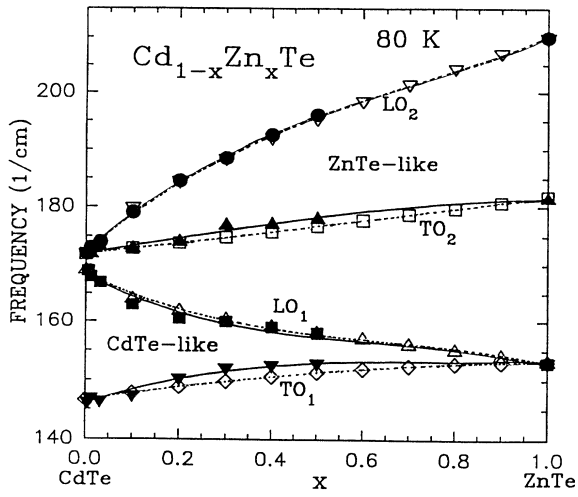

FIG. 3. Variation of LO and TO frequencies in $Cd_{1-x}Zn_xTe$ as a function of composition x. Solid lines are the least-squares fits to the experimental data (solid symbols), whereas the dotted lines are the fits from an MREI model (open symbols) with parameter values of Table I.

For the four samples with $x<0.1$ the second-order LO phonons ($2LO_1$, LO_1+LO_2, and $2LO_2$) also appeared between 310 and 380 cm^{-1}. Their intensities were comparable to the first-order features, due to the incoming resonance at the 488-nm excitation. For samples with $x=0.2-0.5$, the LO_1 becomes weak. However, the LO_2 mode still possesses a clear band shape. The second-order phonon features are almost nonobservable for these samples. For pure ZnTe, the first-order Raman-active LO phonon (~ 210 cm^{-1}) is in excellent agreement with the inelastic neutron scattering data.[20,21] We also observed a second-order (2LO) phonon feature near 420 cm^{-1}. Results of IR and Raman-scattering experiments reported in Figs. 1 and 2 for the low Zn composition have demonstrated characteristics of the lattice dynamics of $Cd_{1-x}Zn_xTe$ in terms of being a two-mode system (see Fig. 3).

III. THEORETICAL CONSIDERATIONS

The dynamical properties of crystalline solids are generally considered in terms of the response of the medium to the excitation from an electromagnetic wave. The response may be elastic or inelastic and can be characterized either in terms of a dielectric function or in terms of a scattering cross section.[16] Here, we are concerned with the effects of defects on two typical response functions: (i) the dielectric susceptibility tensor $\{\chi_{\alpha\beta}\}$, and (ii) the scattering tensor $\{i_{\alpha\gamma\beta\lambda}\}$. In terms of these response functions the optical properties of $Cd_{1-x}Zn_xTe$ alloys are studied using an averaged-t-matrix formalism.

A. Optical response function: Infrared reflectivity

The theoretical interpretation of the IR reflectivity-absorption data requires the computation of the dielectric function $\epsilon(\omega,\mathbf{q})$ from a reliable scheme. This function is generally divided into *two* parts: (i) the ionic $\{\epsilon_i\}$ part, and (ii) the electronic $\{\epsilon_e\}$ part,

$$\epsilon(\omega,\mathbf{q})=\epsilon_i(\omega,\mathbf{q})+\epsilon_e(\omega,\mathbf{q}) \ . \tag{1}$$

The division is justified by the fact that the singularities of ϵ_i lie in a range of energies much lower than the range of energies of the electronic (ϵ_e) singularities, except for critical cases (such as zero gap semiconductors). Infrared absorption and Raman scattering provide two complementary techniques for studying the long-wavelength optical phonons ($\mathbf{q}=0$) in compound semiconductors. In the presence of a defect the $\mathbf{q}=0$ selection rule is relaxed and the electromagnetic radiation is able to interact with other polar modes of the imperfect lattice. The coupling of an electromagnetic field $\mathbf{E}(t)$ $[\underset{\lim\delta\to 0}{=}\mathbf{E}_0\exp(-i\omega+\delta)t]$ with electric dipole moment $\mathcal{M}$ of the crystal introduces a perturbation $\mathcal{H}_{\rm int}$ $[=-\mathcal{M}\cdot\mathbf{E}(t)]$. By solving the Schrödinger equation with a perturbed Hamiltonian $\mathcal{H}$ $(=\mathcal{H}_0+\mathcal{H}_{\rm int})$, one can obtain the expectation value of the electric dipole moment $\langle\mathcal{M}_\alpha\rangle$ produced by the lattice vibrations. Since the dipole moment is linearly dependent on E, it can be expressed in terms of the dielectric susceptibility $\chi(\omega)$ tensor as

$$\langle\mathcal{M}_\alpha\rangle=\sum_\beta\chi_{\alpha\beta}E_\beta \ . \tag{2}$$

If the Kubo[22] formalism is used, the dielectric susceptibility per unit volume takes the form

$$\chi_{\alpha\beta}(\omega)\underset{\lim\delta\to 0}{=}\frac{i}{\hbar V}\int_0^\infty dt\langle[\mathcal{M}(t),\mathcal{M}(0)]\rangle_T\exp(i\omega-\delta)t \ . \tag{3}$$

The term $\mathcal{M}$ can be expanded in terms of the ionic displacements ($\mathbf{u}$) from equilibrium position as

$$\mathcal{M}_\alpha=\mathcal{M}_\alpha^0+\sum_{l\kappa\beta}\mathcal{M}_{\alpha\beta}(l\kappa)u_\beta(l\kappa)+\sum_{l\kappa\beta l'\kappa'\gamma}\mathcal{M}_{\alpha\beta\gamma}(l\kappa,l'\kappa')\mu_\beta(l\kappa)u_\gamma(l'\kappa')+\cdots \ . \tag{4}$$

In Eq. (4), the first term $\mathcal{M}_\alpha^0$ which is responsible for the permanent dipole moment vanishes for the case of cubic crystals; the second term $\mathcal{M}_{\alpha\beta}(l\kappa)$ $[=\partial\mathcal{M}_\alpha/\partial u_\beta(l\kappa)|_0]$, which has the significance of representing an effective charge tensor ($\mathbf{Z}$), gives rise to the one-phonon absorption contribution to the far-infrared dielectric constant; and the third term $\mathcal{M}_{\alpha\beta\gamma}(l\kappa,l'\kappa')$ $[=\partial^2\mathcal{M}_\alpha/\partial u_\beta(l\kappa)\partial u_\gamma(l'\kappa')|_0]$ is responsible for the second-order phonon absorption contribution to the dielectric constant, etc. For the first-order electric dipole moment, the required susceptibility involves a displacement-displacement $\{\langle\langle u_\alpha(l\kappa,t)u_\beta(l'\kappa)\rangle\rangle\}$ correlation function which can readily be calculated via the Green's function formulation as

$$\chi_{\alpha\beta}\underset{\lim\delta\to 0}{=}-\frac{1}{V}\sum_{l\kappa\alpha l'\kappa'\beta}Z_\alpha(l\kappa)Z_\beta(l'\kappa')G_{\alpha\beta}(l\kappa;l'\kappa',\omega+i\delta) \ , \tag{5}$$

where $Z_\alpha(l\kappa)$ is the effective charge of the $(\alpha,l\kappa)$ atom. In writing Eq. (5), we used Fourier transformation with respect to time and related the double-time Green's function of the displacement operators to a classical function

$$G_{\alpha\beta}(l\kappa;l'\kappa',\omega)=\frac{1}{\hbar}\int_{-\infty}^{\infty}\langle\langle u_\alpha(l\kappa,t)u_\beta(l'\kappa')\rangle\rangle\exp(i\omega t)dt \ . \tag{6}$$

The above Green's function of the imperfect crystal Hamiltonian $\mathcal{H}$ satisfies the equation of motion (in matrix notation)

$$\mathbf{G}^{-1}(\omega)=\mathbf{M}\omega^2-\Phi \tag{7}$$

and a similar equation $[\mathbf{G}_0^{-1}(\omega)=\mathbf{M}_0\omega^2-\Phi_0]$ exists for the perfect crystal with Hamiltonian $\mathcal{H}_0$. Here, the terms Φ_0 (Φ), and $\mathbf{M}_0$ ($\mathbf{M}$) are, respectively, the force constant and mass matrices for the perfect (imperfect) crystal. The well-known Dyson equation relating $\mathbf{G}$ and $\mathbf{G}_0$,

$$\mathbf{G}(\omega)=G_0(\omega)+\mathbf{G}_0(\omega)\Lambda^l(\omega)\mathbf{G}(\omega) \ , \tag{8}$$

can be easily iterated to give

$$\mathbf{G}(\omega)=\mathbf{G}_0(\omega)+\mathbf{G}_0(\omega)\Lambda^l(\omega)\mathbf{G}_0(\omega)+\mathbf{G}_0(\omega)\Lambda^l(\omega)\mathbf{G}_0(\omega)\Lambda^l(\omega)\mathbf{G}_0(\omega)+\cdots \ . \tag{9}$$

This expansion is trivially summed exactly to give

$$\mathbf{G}(\omega)=\mathbf{G}_0(\omega)+\mathbf{G}_0(\omega)\mathbf{t}^l(\omega)\mathbf{G}_0(\omega) \ , \tag{10}$$

where the t matrix is defined as

$$\mathbf{t}^l(\omega)=\Lambda^l(\omega)[\mathbf{I}-\mathbf{G}_0^l(\omega)\Lambda^l(\omega)]^{-1} \ . \tag{11}$$

Here the elements of the perfect lattice Green's function are restricted to those sites about l where Λ^l is nonzero. If Λ^l is large enough, corresponding to a light impurity atom or to a strong harmonic coupling to the impurity, then there will be poles of $\mathbf{t}^l$ corresponding to the zeros

$$\mathrm{Re}[\mathbf{I}-\mathbf{G}_0^l(\omega)\Lambda^l(\omega)]=\mathbf{0} \ , \tag{12}$$

at frequencies above the host frequency spectrum. On the other hand, if the impurity is very heavy or the impurity coupling is very weak, there will be a low-frequency resonance in $\mathbf{t}^l$ corresponding to resonant impurity vibrations. Such a single impurity mode appears in the frequency spectrum as a sharp peak. For the case of a pair of defects at sites l and l'; the solution for $\mathbf{t}_{ll'}$ can be carried out exactly with similar results.

To treat the dynamical behavior of $Cd_{1-x}Zn_xTe$ mixed crystals for finite composition x, the above formalism of single-pair impurity vibrations should be extended for random disordered systems by using a configurational average technique. The average Green's function for a disordered system can be written as[16]

$$\langle \mathbf{G} \rangle^{-1} = [\mathbf{G}_0]^{-1} + \Sigma \ , \tag{13}$$

where the self-energy term Σ plays the role of an effective perturbation. It can be related to the average $\mathbf{T}$ matrix by

$$\Sigma = [\mathbf{I} + \langle \mathbf{T} \rangle \mathbf{G}_0]^{-1} \langle \mathbf{T} \rangle \ . \tag{14}$$

In a multiple-scattering approach

$$\langle \mathbf{T} \rangle = \sum_i \langle \mathbf{T}_i \rangle \tag{15}$$

and

$$\begin{aligned} \langle \mathbf{T}_i \rangle &= \langle (\mathbf{I} + \sum_{i' \neq i} \mathbf{T}_i, \mathbf{G}_0) \mathbf{t}_i \rangle \\ &= \left[\mathbf{I} + \sum_{i' \neq i} \langle \mathbf{T}_{i'} \rangle \mathbf{G}_0 \right] \langle \mathbf{t}_i \rangle \\ &\quad + \left\langle \sum_{i' \neq i} (\mathbf{T}_i - \langle \mathbf{T}_{i'} \rangle)(\mathbf{t}_i - \langle \mathbf{t}_{i'} \rangle) \right\rangle , \end{aligned} \tag{16}$$

where

$$\mathbf{t}_i = \Lambda_i (\mathbf{I} - \mathbf{G}_0 \Lambda_i)^{-1} \ , \tag{17}$$

describes single-site scattering at the ith defect of the phonon wave scattered by the other defects. In Eq. (16) the first term represents the scattering of an average incident wave by an atom with an average t matrix. The second term takes into account the correlation between fluctuations in the incident wave and in the atomic t matrix. In a single-site approximation one neglects the correlation term. This further simplifies Σ to the following form:

$$\Sigma = \sum_i \langle \mathbf{t}_i \rangle [\mathbf{I} + \mathbf{G}_0 \langle \mathbf{t}_i \rangle]^{-1} \ . \tag{18}$$

For mass disorder Λ is diagonal in the site representation and so is $\mathbf{t}$. It should be pointed out that the above relations hold even if $\mathbf{G}_0$ represents the Green's function of an arbitrary reference crystal. The standard choice in ATM has been to treat the latter as a periodic lattice with cation masses equal to the weighted average between Cd and Zn atoms. In this case Σ is exact at both limits of the composition range, if the first-order expansion[23] in the defect concentration is carried out. Using the relationship between the dielectric constant and the susceptibility, one may obtain $\epsilon(\omega)$ in the spectral region of interest and consequently the dynamical properties of ternary $Cd_{1-x}Zn_xTe$ alloys.

C. Phonon-assisted Raman scattering

The description of impurity-induced first-order Raman scattering in mixed crystals may also be represented in the ATM formalism. In this formalism the intensity of linearly polarized Raman scattering for unit solid angle Ω and for unit frequency shift ω_s $(=\omega_i + \omega)$ is given by[17]

$$\mathbf{I}(\omega_i, \omega_s : \Omega) \sim \frac{\hbar \omega_i^4}{2\pi^2 c^3} \sum_{\alpha\beta\gamma} \sum_{\alpha'\beta'\gamma'} \sum_{l\kappa l'\kappa'} n_\alpha n_{\alpha'} E_\beta E_{\beta'}^* \eta(\omega_i - \omega_2) \langle \mathcal{P}_{\alpha\beta,\gamma}(l\kappa) \mathcal{P}_{\alpha'\beta',\gamma'}(l'\kappa')_{\lim_\delta \to 0} \mathrm{Im} \langle l\kappa\gamma | \mathbf{G}(\omega) | l'\kappa'\gamma' \rangle \rangle \ ,$$

where n is the thermal occupation number and c is the speed of light. In Eq. (19), the polarizability tensor due to lattice vibrations is expanded as a function of ionic displacements $\mathbf{u}$ and the only terms $\mathcal{P}_{\alpha\beta,\gamma}(l\kappa)$ describing first-order Raman scattering have been retained. It is worth pointing out that the intensity depends upon the direction of the electric field for the incoming (E_β) and the outgoing $(E_{\beta'}^*)$ photons.

IV. NUMERICAL COMPUTATIONS AND RESULTS

A. Local structure of $Cd_{1-x}Zn_xTe$ alloys

Recent extended x-ray-absorption fine-structure (EXAFS) measurements[15] made on ternary-alloy $Cd_{1-x}Zn_xTe$ samples have clarified the local arrangements of the nearest-neighbors (NN) and the next-nearest neighbors (NNN). It is found that the anion-cation bond lengths do not follow Vegard's law[24] but remain almost unchanged in comparison with those of the pure materials. The EXAFS data are interpreted by using a simple but *first-principles* bond-orbital model.[7] From the minimum of the calculated total energy in the BOM, one can estimate the lattice distortion and hence the change in NN bond lengths caused by the Zn/Cd defects in the CdTe/ZnTe lattice. For distribution of the NN distances in ternary $Cd_{1-x}Zn_xTe$ alloys, the theoretical results are displayed in Fig. 4 as a function of composition x. Comparison of the calculation with the existing EXAFS data reveals that the distributions of the anion-cation bond lengths are bimodal and that their values as a function of

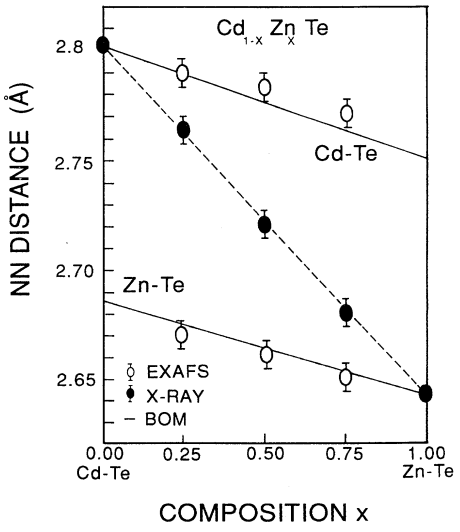

FIG. 4. EXAFS data for the distribution of nearest-neighbor distances in ternary allows as a function of the composition x.

x are closer to those of the reference binary compounds than to the average distance measured by x-ray diffraction.

B. Two-component phonon structure

The composition dependence of the far-infrared reflectivity spectra in $Cd_{1-x}Zn_xTe$ alloys was measured and the preliminary results at low temperatures were reported earlier.[14] The Kramers-Krönig integrations were used before fitting reflectivity spectra to the dynamic dielectric function ϵ. The peaks in $\mathrm{Im}(\epsilon)$ and in $\mathrm{Im}(-1/\epsilon)$ gave the frequencies of the transverse-optical (TO) and the longitudinal-optical (LO) phonon modes, respectively. The LO phonons obtained from Kramers-Krönig integrations are found to be only slightly different from those derived from the Raman-scattering measurements. In Fig. 3, we have displayed the room-temperature infrared TO frequencies and the Raman LO frequencies for $Cd_{1-x}Zn_xTe$ as a function of x. As for $Cd_{1-x}Hg_xTe$, our results for $Cd_{1-x}Zn_xTe$ have exhibited a two-component phonon structure and are consistent with similar data reported by other groups. Unlike other two-mode ternary systems,[12] in which one mode's TO frequency increases with x and the other decreases, in $Cd_{1-x}Zn_xTe$ both frequencies are seen to increase (see Fig. 3) with composition.

A modified random-element-isodisplacement (MREI) model[25] is used, in which the three force constants (f_{CdTe}, f_{ZnTe}, and f_{CdZn}) and θ (see Table I) are allowed to vary, to obtain the best fit to the observed phonon data. Although an excellent agreement was achieved with the experimental results for the variation of optical phonon frequencies in $Cd_{1-x}Zn_xTe$, the success of this study has been confined mainly to the long-wavelength (near $\mathbf{q}=\mathbf{0}$) regime. In the ATM formalism, on the other hand, the numerical simulation of the density of states for the imperfect system provides us with a complicated but meaningful profile of the impurity-induced spectra both in the optical- and acoustical-phonon frequency region (see Fig. 5). In such calculations, we employed the bulk CdTe and ZnTe phonons generated by a rigid-ion model with parameter values from Ref. 19. The involved Green's functions were numerically obtained by performing a root-sampling technique considering 64 000 $\mathbf{q}$ points in the Brillouin zone. A small imaginary part was added to the frequency in order to smooth out the numerical fluctuations. In $Cd_{1-x}Zn_xTe$, clearly the calculated disorder-activated transverse-acoustic (DATA), longitudinal-acoustic (DALA), and optic (DAO) phonon-mode structures are very well described by the ATM. In the extreme limits of the composition x, the theory displays the correct shift in frequencies, and the calculated values of impurity modes agree remarkably well with the experimental data. Moreover, the line shapes in disordered materials are seen to be rather similar to the calculated one-phonon density of states.

TABLE I. MREI model parameters in the notations of Ref. 25 used to explain the observed two-mode behavior by IR and Raman spectroscopy (this study) in $Cd_{1-x}Zn_xTe$ ($AB_{1-x}C_x$, with A = Te, B = Cd, and C = Zn) ternary alloys.

$\epsilon_\infty\, AB$	$=7.3$
$\omega_{TO}\, AB$	$=146.7\ \mathrm{cm}^{-1}$
$\omega_{LO}\, AB$	$=169\ \mathrm{cm}^{-1}$
$\omega^{AB:C}$	$=146.7\ \mathrm{cm}^{-1}$
a_0^{AB}	$=6.481$ Å
ϵ_∞^{AC}	$=7.182$
ω_{TO}^{AC}	$=182\ \mathrm{cm}^{-1}$
ω_{LO}^{AC}	$=210\ \mathrm{cm}^{-1}$
$\omega^{AC:B}$	$=153(?)\ \mathrm{cm}^{-1}$
a_0^{AC}	$=6.1037$ Å
F_{AB0}	$=0.955\times10^5$ dyn/cm
F_{AC0}	$=0.850\times10^5$ dyn/cm
F_{BC0}	$=0.290\times10^5$ dyn/cm
Z^{AB}	$=0.67e$
Z^{AC}	$=0.65e$
θ	$=-0.25$

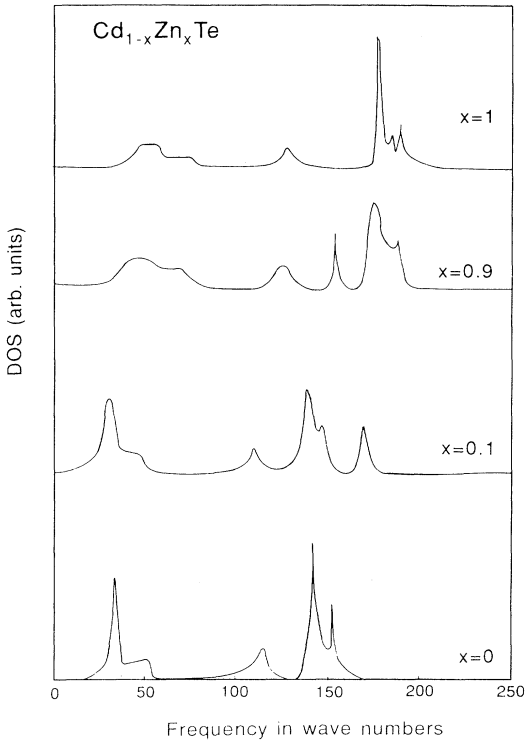

FIG. 5. Calculated phonon density of states for the $Cd_{1-x}Zn_xTe$ homogeneous alloys for different Zn compositions obtained using an average-t-matrix approximation.

V. DISCUSSION AND CONCLUSIONS

We have combined infrared and Raman methods to study the transverse- and longitudinal-optical phonons in a variety of bulk $Cd_{1-x}Zn_xTe$ samples (with compositions over the range $x=0.005$–0.5, and 1). The samples used in the present investigations were grown by the two-zone Bridgman method. Our experimental results confirm that, within a two-mode behavior, both the

CdTe- and ZnTe-like TO mode frequencies increase with x, unlike any other II-VI ternary compounds with known phonon modes. The infrared spectra show signs of clustering behavior like that seen in MCT.[26] It is not clear to us why Olego, Raccah, and Faurie[13] observed a constant CdTe-like TO frequency versus x for their $Cd_{1-x}Zn_xTe$/GaAs films. One possibility is that the stress from the lattice mismatch between film and substrate (10–14 %, depending on the x value) influences the TO frequencies. The other possibility is that the TO modes are not sufficiently sharp in Raman data to give reliable frequencies.

An MREI model, with the parameter values given in Table I, provided excellent fits to the optical phonons. Different criteria that favor the various phonon mode-behavior patterns in mixed ternary $A_{1-x}B_xC$ alloys have been proposed in the literature.[18] Based on our comprehensive lattice-dynamical study we suggest that the two-mode pattern is typical of those ternary compounds for which the optical bands of the binaries (AC and BC) do not overlap (see the optical-phonon densities of states of CdTe and ZnTe in Fig. 5) and where, near the extremes of the composition range, the impurity mode of the minority ions lies well outside the restrahlen peak of the host crystal. In this context, a few points are worth mentioning here: In a linear-diatomic chain model, if the highest and the lowest optical frequencies of the end-member compounds (AC and BC) are calculated by using the same force constant values, one simply attains the mass criterion for the two-mode behavior $m_A^{-1} < m_B^{-1} + m_C^{-1}$ proposed by Chang and Mitra.[27] In the actual lattice-dynamical study, however, the density of states (DOS's) collects contributions from the entire Brillouin zone. Thus, the dispersion and linewidth of the normal modes affect heavily the resulting spectral DOS. As the translational symmetry of the host crystal is destroyed by the presence of defects, the notion of a dispersion relation and of a well-defined phonon wave vector loses its meaning. The density of the vibrational states, however, remains a relevant concept. In the ATM formalism, although the numerical simulation of the DOS for imperfect systems is complicated, it provides a meaningful profile of the impurity-induced spectra both in the optical- and the acoustical-phonon frequency region (see Fig. 5). One of the most important features of the ATM theory is that with a proper choice of the perturbation, such a profile can be obtained in different irreducible representations of the point-group symmetry of the imperfect crystal. If polarization dependent Raman data is known, this profile will facilitate comparison between theoretical and experimental results on the vibrational features. Unfortunately, in $Cd_{1-x}Zn_xTe$ no such data exist. A study is now underway, using Raman scattering in different geometries for detailed polarization-selection-rule analyses, and will be reported elsewhere. Based on our calculations and group-theoretical analysis, we suggest that the gap mode in ZnTe:Cd system lies at a relatively higher frequency ~ 153 cm^{-1} than reported in earlier studies. This mode exhibits a triply degenerate F_2 vibrational state and should be detected both by IR and Raman-scattering spectroscopy in samples with low Cd composition. It is brought to our attention that a recent infrared reflectivity work by Granger, Marqueton, and Triboulet[28] in $Cd_{1-x}Zn_xTe$ for $x > 0.5$ has indeed confirmed our theoretical prediction for the gap mode.

ACKNOWLEDGMENTS

The authors gratefully acknowledge useful discussions on the subject matter with Professor S. Perkowitz of Emory University, Atlanta, Georgia. Part of the work performed by D.N.T. at the Wright Laboratories, Solid State Electronics Directorate, WP AFB, Ohio was supported by the National Research Council Associateship program.

*Permanent address.

[1]See, for example, R. Dornhaus and G. Nimitz, in *Narrow Gap Semiconductors,* edited by G. Höhler and E. A. Niekisch (Springer, Berlin, 1983), pp. 119–300.

[2]See, for example, *Proceedings of the NATO Workshop on Narrow Gap Semiconductors* [Semicond. Sci. Technol. **6**, 12C (1991)].

[3]W. E. Spicer, J. A. Silberman, J. Morgan, I. Lindan, J. A. Wilson, A. B. Chen, and A. Sher, Phys. Rev. Lett. **49**, 948 (1982).

[4]A. B. Chen, A. Sher, and W. E. Spicer, J. Vac. Sci. Technol. A **1**, 1674 (1983).

[5]A. Sher, A. B. Chen, and M. van Schilfgaarde, J. Vac. Sci. Technol. A **4**, 1965 (1986).

[6]A. Sher, A. B. Chen, W. E. Spicer, and C. K. Shih, J. Vac. Sci. Technol. A **3**, 105 (1985).

[7]D. N. Talwar, K. S. Suh, and C. S. Ting, Philos. Mag. B **56**, 593 (1987).

[8]A. Laugier, Rev. Phys. Appl. **8**, 259 (1973).

[9]H. Harada and S. Narita, J. Phys. Soc. Jpn. **30**, 1628 (1970).

[10]L. K. Vodop'yanov, E. A. Vinogradov, A. M. Blinov, and V. A. Rukavishnikov, Fiz. Tverd. Tela (Lenningrad) **14**, 268 (1972) [Sov. Phys. Solid State **14**, 219 (1972)].

[11]E. A. Vinogradov and L. K. Vodop'yanov, Fiz. Tverd. Tela (Lenningrad) **17**, 3161 (1975) [Sov. Phys. Solid State **17**, 2088 (1976)].

[12]Landolt-Börnstein, *Numerical Data and Functional Relationships in Science and Technology,* edited by O. Madelung, Landolt-Bornstein, New Series, Group III, Vol. 22, Pt. a (Springer-Verlag, Berlin, 1987), p. 312.

[13]D. J. Olego, P. M. Raccah, and J. P. Faurie, Phys. Rev. B **33**, 3819 (1986).

[14]S. Perkowitz, L. S. Kim, Z. C. Feng, and P. Becla, Phys. Rev. B **42**, 1455 (1990).

[15]N. Motta, A. Balzarotti, P. Letardi, A. Kisiel, M. T. Czyzyk, M. Zimnal-Starnawska, and M. Podgorny, Solid State Commun. **53**, 509 (1985).

[16]See, for example, M. Bernasconi, in *Phonons: Theory and Experiment III,* edited by P. Brüesch (Springer, Heidelberg, 1987); D. W. Taylor, in *Optical Properties of Mixed Crystals,* edited by R. J. Elliott and I. P. Ipatova (North-Holland, Amsterdam, 1988), p. 35.

[17]M. Bernasconi, L. Colombo, L. Miglio, and G. Benedek, Phys.

Rev. B **43**, 14 447 (1991); **43**, 14 457 (1991).
[18]H. Böttger, *Principles of the Theory of Lattice Dynamics* (Academic, Berlin, 1983).
[19]P. Plumelle and M. Vandevyver, Phys. Status Solidi B **73**, 271 (1976).
[20]N. Vagelatos, D. Wehe, and J. S. King, J. Chem. Phys. **60**, 3613 (1974).
[21]J. M. Rowe, R. M. Nicklow, D. L. Price, and K. Zanio, Phys. Rev. B **10**, 671 (1974).
[22]R. Kubo, J. Phys. Soc. Jpn. **12**, 570 (1957).
[23]D. N. Talwar and M. Vandevyver, Phys. Rev. B **40**, 9779 (1989).
[24]L. Vegard, Z. Phys. **5**, 17 (1921).
[25]M. Gorska and W. Nazarewicz, Phys. Stat. Solidi B **65**, 193 (1974).
[26]S. P. Kozyrev, L. K. Vodop'yanov, and R. Triboulet, Solid State Commun. **45**, 383 (1983).
[27]I. F. Chang and S. S. Mitra, Adv. Phys. **20**, 359 (1971).
[28]R. Granger, Y. Marqueton, and R. Triboulet, J. Phys. (Paris) **3**, 135 (1993).